Journal of Engineering Mechanics and Machinery (2026)
Clausius Scientific Press, Canada

DOI: 10.23977/jemm.2026.110106
ISSN 2371-9133 Vol. 11 Num. 1

Research on UUV Trajectory Tracking Method under the Fusion Mechanism of Enhanced Gaussian Process and MPC

Xiaolong Fan[1], Xuyu Shen[1], Zhenzhong Chu[1,*], Yushen Duan[1]

[1]*School of Mechanical Engineering, University of Shanghai for Science and Technology, Yangpu, Shanghai, China*

[*]*Corresponding Author: zhenzhongchu@usst.edu.cn*

Keywords: Unmanned Underwater Vehicle, Model Predictive Control, Gaussian Process, Uncertainty

Abstract: This paper addresses the trajectory tracking control problem for Unmanned Underwater Vehicle systems under unknown dynamics and uncertainties. The goal is to develop a model predictive control (MPC) method that does not require an exact mechanistic model, overcoming the challenges posed by model mismatch in complex nonlinear systems. Traditional Gaussian process-based MPC methods, with their multi-input single-output characteristics, can only independently compensate for each model dimension, making it difficult to capture coupling relationships between multiple outputs, limiting control accuracy and robustness. To address this, a multi-output Gaussian process MPC method based on a cooperative regionalized model is proposed. This method uses a unified modeling framework to learn dynamic errors and their structure between the theoretical model and real system, effectively representing output coupling, thus improving tracking performance. Additionally, a stochastic constraint handling strategy based on Gaussian process prediction uncertainty is introduced, converting probabilistic constraints into deterministic convex constraints. This ensures efficient online solving and enhances the system's safe operation in complex environments. Finally, comparative simulations demonstrate that the proposed method outperforms classical Gaussian process MPC in terms of tracking accuracy, dynamic response, and constraint satisfaction.

1. Introduction

With the rapid development of marine resource exploration, environmental monitoring, and deep-sea exploration, the importance of Unmanned Underwater Vehicles (UUVs) in ocean engineering has become increasingly prominent, and their development has become a key direction in this field [1-3]. The trajectory tracking control of UUVs is a core technology for tasks such as marine resource exploration, environmental monitoring, and underwater operations. As the complexity of tasks and accuracy requirements continue to rise, the control system must not only drive the UUV to accurately track time-varying reference trajectories but also maintain robust, safe, and efficient closed-loop performance under multiple challenges such as model uncertainty, strong environmental disturbances,

and system constraints. However, UUV dynamics typically exhibit highly nonlinear, strongly coupled, and uncertain parameters, making it difficult to obtain an accurate mathematical model through mechanistic modeling [4]. Additionally, external time-varying ocean currents, fluid dynamic coefficient perturbations, and constraints such as actuator saturation further complicate the controller design. Therefore, designing a control method with high tracking accuracy, strong robustness, and the ability to handle state and input constraints under conditions of unknown or significantly uncertain dynamics has become a critical issue in the current UUV control field [5,6].

Model Predictive Control (MPC), due to its explicit handling of multivariable constraints and rolling optimization capability, has received widespread attention in recent years for UUV control [7-9]. However, traditional MPC relies heavily on precise system models, and its performance often deteriorates significantly under model mismatch or environmental disturbances. To address the challenges posed by model uncertainty, data-driven and learning-based control methods have gradually been introduced into the MPC framework [10-12]. Among these, Gaussian Process (GP) regression, with its non-parametric modeling, quantifiable uncertainty, and Bayesian inference advantages, has become an important method for learning the unmodeled dynamics of a system. Hewing et al.[13] used GP to estimate unmodeled dynamics and integrated it with the nominal model to account for uncertainty, thus enhancing control efficiency. Gaussian Process Model Predictive Control (GP-MPC) can effectively enhance the robustness of control for uncertain systems by learning model errors either online or offline. However, existing GP-MPC methods still have significant limitations in underwater vehicle control applications: most studies use single-output Gaussian processes to independently model each state channel, which, while reducing computational load, neglects the inherent dynamic coupling between multiple output variables, leading to missing model information structure and thus limiting further improvements in control accuracy.

To address the above issues, this paper focuses on the multi-output Gaussian Process modeling and probabilistic constraint handling strategy for model-unknown UUV systems, aiming to improve the accuracy, robustness, and safety of trajectory tracking control. This paper proposes a multi-output GP-MPC based on the ICM method, which learns the errors and related structures of each state channel synchronously through a unified model, thereby more comprehensively characterizing the coupled dynamics and improving prediction accuracy. Simultaneously, a stochastic constraint handling strategy based on GP uncertainty is designed, which converts probabilistic safety constraints into deterministic convex constraints, enhancing safety in complex uncertain environments while ensuring online solving efficiency. The proposed method's advantages in tracking accuracy, dynamic response, and constraint satisfaction are validated through comparative simulations.

The main contributions of this paper are as follows:

(1) A state-space equation with four inputs and three outputs is established, which comprehensively considers the impact of external disturbances and other factors on the UUV system, accurately describing the trajectory tracking kinematic characteristics of the UUV.

(2) By introducing a multi-output Gaussian process model extended based on a cooperative regionalized model, a more comprehensive representation of the interdependencies between the states of the control system is achieved.

(3) The probabilistic constraints derived from the variance estimation of the Gaussian process model are transformed into computable convex constraints, reducing the conservativeness associated with MPC control.

This paper first establishes the UUV control problem model, then proposes a multi-output GP modeling approach based on ICM and its integration with MPC. It also presents a strategy for the conversion of probabilistic constraints based on GP uncertainty and efficient optimization techniques. Finally, the method's effectiveness is verified through simulations, and the paper concludes with a summary and an outlook on future research directions.

2. System Model Description

In UUV motion control, trajectory tracking is a key link in achieving path planning and task execution. Due to hydrodynamic effects, the dynamics of UUVs exhibit strong nonlinearity, time-variance, and multivariable coupling characteristics, making the modeling process challenging and directly limiting the controller design and tracking performance [14]. Therefore, research on UUV trajectory tracking control requires the development of a dynamic model that can reasonably represent its horizontal motion characteristics, providing fundamental support for the design and performance analysis of control algorithms.

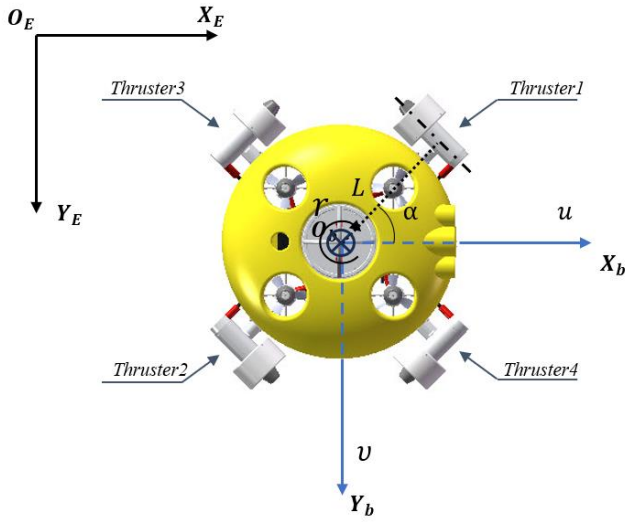

Figure 1. Schematic of the UUV coordinate frames.

The kinematic and dynamic modeling of the UUV is established based on its three degrees of freedom (3-DOF) motion in the horizontal plane. In this study, a body-fixed reference frame, denoted as $X_b - Y_b - O_b$ is adopted. The origin of this coordinate system is located at the center of gravity of the UUV, and the frame is rigidly attached to the vehicle body, as illustrated in Fig.1. Meanwhile, in the inertial earth-fixed reference frame $X_E - Y_E - O_E$, X_E and Y_E denote the true north and true east directions, respectively. The velocity vector of the UUV in the body-fixed reference frame is defined as $\mathrm{v} = [\mathrm{u}, v, r]^T$, which represents the surge velocity, sway velocity, and yaw rate of the UUV, respectively. In the inertial coordinate system, the position and heading of the UUV are defined as $\eta = [x, y, \psi]^T$. Accordingly, the kinematic equations of the UUV can be expressed as follows:

$$\dot{\eta} = \mathrm{R}(\psi)\boldsymbol{v} \tag{1}$$

Here, $\mathrm{R}(\psi)$ denotes the rotation matrix that depends on the heading angle ψ [15]:

$$\mathrm{R}(\psi) = \begin{bmatrix} \cos\psi & -\sin\psi & 0 \\ \sin\psi & \cos\psi & 0 \\ 0 & 0 & 1 \end{bmatrix}$$

In horizontal-plane motion, since the restoring forces are neglected, the dynamic equations can be expressed as follows:

$$M\dot{\boldsymbol{v}} + C(\boldsymbol{v})\boldsymbol{v} + D(\boldsymbol{v})\boldsymbol{v} = \tau \tag{2}$$

Here, $\tau = [F_u, F_v, F_r]^T$ denotes the generalized thrust vector, M represents the inertia matrix including added mass, $C(\boldsymbol{v})$ is the Coriolis and centripetal matrix, and $D(\boldsymbol{v})$ denotes the hydrodynamic damping matrix.

In this study, the generalized thrust of the UUV is generated by four thrusters, and the thrust vector of the thrusters is defined as $\boldsymbol{u} = [u_1, u_2, u_3, u_4]$. The four thrusters are symmetrically arranged, as shown in Fig. 1. According to the geometric configuration of the thrusters, the generalized forces (and moments) acting on the center of gravity in the body-fixed coordinate system can be expressed as follows:

$$\tau = B\boldsymbol{u} \tag{3}$$

Here, the matrix $\boldsymbol{B} \in$ ¡ $^{3\times m}$ denotes the thrust allocation matrix [16], which is derived based on the configuration of the horizontal thrusters shown in Fig. 1 as follows:

$$\boldsymbol{B} = \begin{bmatrix} \cos\boldsymbol{\alpha} & -\cos\boldsymbol{\alpha} & -\cos\boldsymbol{\alpha} & \cos\boldsymbol{\alpha} \\ \sin\boldsymbol{\alpha} & -\sin\boldsymbol{\alpha} & \sin\boldsymbol{\alpha} & -\sin\boldsymbol{\alpha} \\ \boldsymbol{L} & \boldsymbol{L} & -\boldsymbol{L} & -\boldsymbol{L} \end{bmatrix}$$

Here, α denotes the thruster configuration angle, and L represents the distance from the center of the UUV to each thruster.

To address the challenges arising from the combined effects of modeling uncertainties and external disturbances in horizontal-plane trajectory tracking control, it is assumed that the inertia matrix, Coriolis matrix, and damping matrix consist of nominal components and uncertain components, i.e., $M = \bar{M} + \Delta M$, $C = \bar{C} + \Delta C$, and $D = \bar{D} + \Delta D$. Here, $\bar{M}$, $\bar{C}$ and $\bar{D}$ denote the nominal system matrices, whereas ΔM , ΔC and ΔD represent the uncertainty terms induced by unmodeled dynamics. Based on this assumption, the actual horizontal-plane motion model of the UUV can be expressed as follows:

$$\begin{aligned} \dot{\eta} &= R(\psi)v \\ \dot{\mathbf{v}} &= M^{-1}\left(\tau - \left(\bar{C}(\mathbf{v}) + \bar{D}(\mathbf{v})\right)\mathbf{v}\right) + \Delta \end{aligned} \tag{4}$$

Here, $\Delta = \frac{1}{\bar{M}}\left(\Delta M\,\dot{\boldsymbol{v}} + \left(\Delta C(\boldsymbol{v}) + \Delta D(\boldsymbol{v})\right)\boldsymbol{v} + \tau_w\right)$ denotes the lumped disturbance induced by model parameter uncertainties and time-varying disturbances.

By combining (3) and (4), the dynamic model of the UUV can be established as follows:

$$\begin{aligned} \dot{\boldsymbol{x}} &= \begin{bmatrix} R(\psi)\boldsymbol{v} \\ M^{-1}\left(\boldsymbol{B}\,\boldsymbol{u} - \boldsymbol{C}(\boldsymbol{v})\boldsymbol{v} - \boldsymbol{D}(\boldsymbol{v})\boldsymbol{v}\right) + \Delta \end{bmatrix} \\ &= f(\boldsymbol{x}, \boldsymbol{u}) + \%\Delta \end{aligned} \tag{5}$$

Here, the state vector is defined as $\boldsymbol{x} = [x, y, \psi, \mathrm{u}, v, r]^T$, and the control input vector is defined as $\boldsymbol{u} = [u_1, u_2, u_3, u_4]^T$. The term $f(\cdot)$ represents the nominal model of the system, while the uncertain component is denoted by $\%\Delta = [0, \Delta]^T$.

To address the aforementioned issues, this paper incorporates thruster chance constraints into the control design within a learning-based MPC framework. In doing so, accurate trajectory tracking is ensured while achieving global optimization of thruster performance.

3. Model Predictive Control Based on Gaussian Processes

3.1 Model Predictive Control

To more accurately characterize this class of algorithms and comprehensively account for various influencing factors in UUV motion control, the state-space model of the UUV is formulated as follows:

$$\dot{\boldsymbol{x}} = f(\boldsymbol{x},\boldsymbol{u}) + \mathrm{L}(\boldsymbol{x},\boldsymbol{u}) + w \tag{6}$$

Here, $\boldsymbol{u} = \left[u_1, u_2, u_3, u_4\right]^T \in \mathrm{U}$ denotes the control input, f represents the nominal dynamic model of the system, and L denotes the unmodeled dynamics. The constraints on the system states and control inputs are specified in $\boldsymbol{x} \in \mathrm{X}$, $\boldsymbol{u} \in \mathrm{U}$, respectively, while $w = \tilde{\Delta}$ represents unknown disturbances. The set U is a convex set containing the origin, and X is a connected closed set that includes the origin. The unmodeled dynamics L are assumed to be bounded.

For the purpose of controller design, the nominal model is defined as follows:

$$\bar{\boldsymbol{x}}(k+1) = f\left(\bar{\boldsymbol{x}}(k), \bar{\boldsymbol{u}}(k)\right) \tag{7}$$

Here, $\bar{x}$ and $\bar{u}$ denote the state and input of the nominal model, respectively. The learning-based model is given by the following expression:

$$\begin{aligned} \boldsymbol{x}(k+1) = {} & f\left(\boldsymbol{x}(k), \boldsymbol{u}(k)\right) \\ & + \mathrm{L}\left(\boldsymbol{x}(k), \boldsymbol{u}(k)\right) + w(k) \end{aligned} \tag{8}$$

Here, x and u denote the state and input of the learning-based model, respectively.

To enhance the tracking performance with respect to the reference trajectory and improve the smoothness of the closed-loop response, the following cost function is constructed:

$$\mathrm{J}\ \left(\boldsymbol{x}, k, \boldsymbol{u}, \boldsymbol{x}_0\right) @ V_f\left(\boldsymbol{x}(N)\right) + \sum_{k=0}^{N-1} \mathrm{l}\left(\boldsymbol{x}(k), \boldsymbol{u}(k)\right) \tag{9}$$

Here, N denotes the prediction horizon length, and $\mathrm{l}(\boldsymbol{x},\boldsymbol{u})$ is the stage cost function defined by $\mathrm{l}(\boldsymbol{x},\boldsymbol{u}) @ \boldsymbol{x}^T Q \boldsymbol{x} + \boldsymbol{u}^T R \boldsymbol{u}$, where $Q > 0, \quad R > 0$ is a positive definite weighting matrix. The terminal cost function is defined as $V_f(\boldsymbol{x}) = \boldsymbol{x}^T P \boldsymbol{x}$, with $P > 0$ being the terminal weighting matrix. Furthermore, the control inputs over the entire prediction horizon are defined as the control sequence:

$$\boldsymbol{u}(x, k, x_0) @ \left\{\boldsymbol{u}(x, 0, x_0), \boldsymbol{u}(x, 1, x_0), \ldots, \boldsymbol{u}(x, N-1, x_0)\right\} \tag{10}$$

3.2 Gaussian Process

To overcome the dependence of conventional adaptive predictive control on inaccurate models and its tendency to fall into local optima, it is recognized that the deviation between the actual system output and the predicted output arises from model mismatch and measurement noise. To more clearly characterize the underlying relationship, the interaction between the system prediction error and the state and input variables is described as follows:

$$\begin{aligned} d(k) &= \mathrm{L}(\boldsymbol{x}(k), \boldsymbol{u}(k)) + w(k) \\ &= \boldsymbol{x}(k+1) - f(\boldsymbol{x}(k), \boldsymbol{u}(k)) \end{aligned} \tag{11}$$

To enhance the optimization performance of predictive control for the UUV, uncertainties in both state measurements and input measurements are considered in the modeling process. The model takes the state–input measurement pair as the input, denoted by $z(k) := \left[\boldsymbol{x}(k)^T, \boldsymbol{u}(k)^T \right]^T \in \mathrm{Z}$, $k = 1, \ldots, M$, and the corresponding training dataset is defined as follows:

$$\mathrm{D} = \left\{ \left(z(k), d(k) \right) \mid k = 1, \ldots, M \right\} \tag{12}$$

GP is characterized by a mean function $m(\cdot)$ and a covariance function $k(\cdot,\cdot)$, which are defined as follows:

$$\begin{aligned} m(z) &= \mathrm{E}[\mathrm{Z}] \\ k(z, z') &= \mathrm{E}[(z - m(z'))(z' - m(z'))] \\ &= \mathrm{E}[z - m(z')]\mathrm{E}[z' - m(z')] \end{aligned} \tag{13}$$

Here, the covariance function $k(z, z')$ is used to characterize the correlation structure between function values at different input points.

In this study, the prediction error vector d is modeled as following a Gaussian distribution:

$$d \sim \mathrm{N}\left(m(z), k(z, z') + \sigma_w^2 I \right) \tag{14}$$

Here, σ_w^2 represents the noise level in the observations, and I is the identity matrix. For simplicity of derivation, the prior GP mean function is set to zero, and the model is inferred and updated solely through the covariance function [17].

Furthermore, the choice of the kernel function has a critical impact on the modeling performance of the GP. In this paper, the squared exponential kernel function is adopted, which assumes that the correlation between any two points decays as the distance between their inputs increases:

$$k(\mathrm{z}_i, \mathrm{z}_j) = \sigma_f^2 \exp\left(-\frac{\| \mathrm{z}_i - \mathrm{z}_j \|}{2\lambda^2} \right) \tag{15}$$

By adjusting the length-scale hyperparameter λ and the signal variance σ_f^2, the correlation between data points can be modulated accordingly.

Remark 1: Classical GP typically assumes that each output is mutually independent. Therefore, it is more suitable for multi-input single-output scenarios and is not well suited to directly capture the coupling relationships among multiple outputs in multi-output cases.

Remark 2:GP regression training requires estimating the set of kernel hyperparameters $\eta = [\lambda,\ \sigma_f]$ by maximizing the log-marginal likelihood. However, the estimation of the mismatch model also depends on the noise variance σ^2, which is typically unknown. In practice, the mismatch model can first be preliminarily fitted using the least-squares method, and the noise variance can then be estimated from the sample variance of the residuals.

Given the training data D, the observation z and the corresponding function value d at a new data point L are jointly distributed according to a multivariate Gaussian distribution as follows:

$$\begin{bmatrix} d \\ \mathrm{L} \end{bmatrix} \sim \mathrm{N}\left(\alpha, \beta \right) \tag{16}$$

Here, $\alpha = \begin{bmatrix} m(\mathrm{Z}) \\ m(z) \end{bmatrix}$, $\beta = \begin{bmatrix} K(\mathrm{Z},\mathrm{Z}) + \sigma_w^2 I & K(\mathrm{Z},z) \\ K(z,\mathrm{Z}) & K(z,z) \end{bmatrix}$, and $K(\mathrm{Z},\mathrm{Z})$ denote the covariance matrices among the training observations; $K(z,z)$ represents the covariance matrix among the new input points; $K(z,\mathrm{Z})$ is the covariance matrix between the new inputs and the training inputs; and $K(\mathrm{Z},z)$ is the transpose of $K(z,\mathrm{Z})$.

The mean μ^* and covariance function Σ^* of the posterior GP are computed as follows:

$$\begin{aligned} \mu^*(z) &= K(z,\mathrm{Z})\left[K(\mathrm{Z},\mathrm{Z}) + \sigma_w^2 I\right]^{-1} d \\ \Sigma^*(z) &= k(z,z') \\ &\quad - K(z,\mathrm{Z})\left[K(\mathrm{Z},\mathrm{Z}) + \sigma_w^2 I\right]^{-1} K(\mathrm{Z},z') \end{aligned} \tag{17}$$

The above procedure obtains the posterior mean and variance by computing the relevant covariance matrices, thereby providing a robust probabilistic modeling foundation for predictive control optimization in the presence of noise and model uncertainties.

3.3 Multi-Output Gaussian Process Modeling

Within the MPC framework, conventional GP typically adopts independent single-output modeling to reduce computational complexity. However, this approach neglects the correlations among outputs and approximates the covariance matrix as diagonal, making it difficult to capture multivariable coupling and thereby limiting improvements in control performance. In contrast, MOGP construct a richer covariance structure by introducing non-diagonal covariance terms, enabling the modeling of latent correlations among outputs.

Assume that R sample functions $\mathrm{GP}^1(z),\ldots,\mathrm{GP}^R(z) \sim \mathrm{N}(0,k(z,z'))$ are drawn from a Gaussian process $k(z,z')$ generated by the kernel function $\mathrm{N}(0,k(z,z'))$. For the output $d(z)=[d_1(z),\ d_2(z),\ \ldots,\ d_D(z)]$, it is assumed that the corresponding output function can be expressed as a linear combination of these sampled functions as follows:

$$\begin{aligned} d_i(z) &= \phi_i^1 \mathrm{GP}^1(z) + \cdots + \phi_i^R \mathrm{GP}^R(z) \\ &\vdots \\ d_D(z) &= \phi_D^1 \mathrm{GP}^1(z) + \cdots + \phi_D^R \mathrm{GP}^R(z) \end{aligned} \tag{18}$$

Furthermore, a coefficient matrix Γ is introduced to characterize the correlation structure among multiple outputs. Accordingly, we obtain:

$$\Gamma = \begin{bmatrix} \phi_1^1 & \cdots & \phi_1^R \\ \vdots & & \vdots \\ \phi_D^1 & \cdots & \phi_D^R \end{bmatrix}$$

Therefore,

$$\begin{aligned} k\left(\mathrm{GP}(z),\mathrm{GP}(z')\right) &= \mathrm{E}\left[\mathrm{GP}(z)\mathrm{GP}(z')^T\right] \\ -\mathrm{E}\left[\mathrm{GP}(z)\right]\mathrm{E}^T\left[\mathrm{GP}(z')\right] &= \Gamma\Gamma^T k(z,z') \end{aligned} \tag{19}$$

Assume that $L=\Gamma^{T}\Gamma$; in this case, the joint distribution at this point is given by:

$$\begin{bmatrix} \mathrm{GP}_1(z) \\ \vdots \\ \mathrm{GP}_D(z) \end{bmatrix} = \begin{bmatrix} \mathrm{GP}_1(z_1) \\ \vdots \\ \mathrm{GP}_1(z_N) \\ \vdots \\ \mathrm{GP}_D(z_1) \\ \vdots \\ \mathrm{GP}_D(z_N) \end{bmatrix} \sim \mathrm{N}\left(\begin{bmatrix} 0 \\ \vdots \\ 0 \end{bmatrix}, L \otimes k \right) \tag{20}$$

To estimate the output correlation structure, a gradient descent method is employed to obtain the maximum likelihood estimate of the correlation matrix. The update rule of the correlation matrix is given by:

$$L(i) = L(i-1) - \tau * \nabla L(i-1) \tag{21}$$

Here, τ denotes the learning rate, and the gradient is taken with respect to the likelihood function relative to the parameters. The value of the gradient can be derived from the log-likelihood function.

Accordingly, the prediction error follows the distribution:

$$d \sim \mathrm{N}\left(m(z), K_{\mathrm{G,G}} + I\sigma^2\right) \tag{22}$$

The posterior predictive mean and variance can be reformulated as follows:

$$\begin{aligned} \mu^{*}(z) &= K_{\mathrm{G,G}}(z,\mathrm{Z})\left[K_{\mathrm{G,G}}(\mathrm{Z},\mathrm{Z}) + \sigma_w^2 I\right]^{-1} d \\ \Sigma^{*}(z) &= k(z,z') - \\ & K_{\mathrm{G,G}}(z,\mathrm{Z})\left[K_{\mathrm{G,G}}(\mathrm{Z},\mathrm{Z}) + \sigma_w^2 I\right]^{-1} K_{\mathrm{G,G}}(\mathrm{Z},z') \end{aligned} \tag{23}$$

3.4 Uncertainty Propagation and Chance Constraints

In the previous section, the MOGP modeling approach for the system's unmodeled dynamics and external disturbances was analyzed. Next, we focus on linearizing the nominal system dynamics around the mean value:

$$f(\boldsymbol{x},\boldsymbol{u}) \approx f\left(\mu^{x},\mu^{u}\right) + \nabla f\left(\mu^{x},\mu^{u}\right)\left(\begin{bmatrix}\boldsymbol{x}\\ \boldsymbol{u}\end{bmatrix} - \begin{bmatrix}\mu^{x}\\ \mu^{u}\end{bmatrix}\right) \tag{24}$$

Accordingly, the predicted mean and variance of the system states can be recursively updated using the following equations:

$$\begin{aligned} \mu^{x}(k+1) &= f\left(\mu^{x}(k),\mu^{u}(k)\right) + \mu^{*}\left(\mu^{x}(k),\mu^{u}(k)\right) \\ \Sigma^{x}(k+1) &= \left[\nabla f\left(\mu^{x}(k),\mu^{u}(k)\right) \quad I\right] \times \\ & \Sigma(k)\left[\nabla f\left(\mu^{x}(k),\mu^{u}(k)\right) \quad I\right]^{T} \end{aligned} \tag{25}$$

Conventional GP-MPC approaches typically impose hard constraints on the outputs. However, under strong uncertainty, this may lead to overly conservative control strategies and even numerical

infeasibility. To address this issue, chance constraints are adopted in place of hard constraints, which are formulated as follows:

$$\begin{aligned} &\Pr\{\boldsymbol{x}(k+i\,|\,k) \le x_{\max}\} \ge \beta, \quad i=1,\ldots,N \\ &\Pr\{\boldsymbol{x}(k+i\,|\,k) \ge x_{\min}\} \ge \beta, \quad i=1,\ldots,N \end{aligned} \tag{26}$$

Here, $\Pr\{A\}$ denotes the probability of event A, and β represents the confidence level required for satisfying the output constraints. Since the system output after linearization can be obtained from a linear prediction model and the unmodeled error is assumed to follow a Gaussian distribution, the chance constraints can be equivalently transformed into deterministic convex constraints with respect to the control inputs, thereby improving online computational efficiency and feasibility.

Because the predicted output can be regarded as a linear transformation of a random variable, the future output prediction follows the Gaussian distribution given by:

$$\boldsymbol{x}(k+i\,|\,k) \sim \mathrm{N}\left(\mu^{+}(k), \Sigma^{+}(k)\right) \tag{27}$$

Here,
$$\mu^{+} = f\left(\mu^{x}(k), \mu^{\boldsymbol{u}}(k)\right) + \mu^{*}\left(\mu^{x}(k), \mu^{\boldsymbol{u}}(k)\right)$$
$$\Sigma^{+} = \left[\nabla f\left(\mu^{x}(k), \mu^{\boldsymbol{u}}(k)\right) \quad I\right] \times \Sigma(k) \left[\nabla f\left(\mu^{x}(k), \mu^{\boldsymbol{u}}(k)\right) \quad I\right]^{T}.$$

By incorporating the predicted distribution of the output into the chance constraints and considering the upper bound constraint, the constraint can be transformed into:

$$\Pr\left\{\frac{\mu^{+}(k) - m(z(k))}{\sqrt{\Sigma^{+}}} \le \frac{x_{\max} - m(z(k))}{\sqrt{\Sigma^{+}}}\right\} \ge \beta \tag{28}$$

Based on the confidence level β, the corresponding value of the inverse cumulative distribution function of the standard normal distribution, denoted by $\Phi^{-1}(\beta)$, can be computed as follows:

$$\frac{x_{\max} - m(z(k))}{\sqrt{\Sigma^{+}}} \ge \Phi^{-1}(\beta) \tag{29}$$

From this, it can be further obtained that:

$$m(z(k)) + \Phi^{-1}(\beta)\sqrt{\Sigma^{+}} \le x_{\max} \tag{30}$$

Within the GP-MPC framework, the system states are required to satisfy the constraints with a prescribed confidence level under an allowable maximum probability of violation.

For the trajectory tracking task, $\boldsymbol{x}_e(k)$ is defined as the deviation between the current state and the desired state. Accordingly, the UUV trajectory tracking optimal control problem based on the MOGP-MPC framework can be formulated as follows:

$$\begin{aligned} &\min_{\{\mu_i^c\}} \ \mathrm{J}\ \left(\boldsymbol{x}_e(k+i|\ k), \boldsymbol{u}(k+i|\ k)\right) \\ &\quad \boldsymbol{x}(k+i+1|\ k) = f\left(\boldsymbol{x}(k+i|\ k), \boldsymbol{u}(k+i|\ k)\right) + d(k+i|\ k), \\ &\quad f\left(\boldsymbol{x}(k+i|\ k), u(k+i|\ k)\right) \approx f\left(\mu^{x}(k+i|\ k), \mu^{\boldsymbol{u}}(k+i|\ k)\right) \\ &\quad + \nabla f\left(\mu^{x}(k+i|\ k), \mu^{\boldsymbol{u}}(k+i|\ k)\right)\left(\begin{bmatrix}\boldsymbol{x}\\ \boldsymbol{u}\end{bmatrix} - \begin{bmatrix}\mu^{x}\\ \mu^{\boldsymbol{u}}\end{bmatrix}\right) \end{aligned} \tag{31}$$

$$
\begin{aligned}
\text{s.t.}\quad & d\left(k+i|\ k\right)\sim \mathrm{N}\left(\mu^{*},\Sigma^{*}\right),\\
& \mu^{+}\left(z_{k}\right)+\Phi^{-1}\left(\beta\right)\sqrt{\Sigma^{+}}\le x_{\max},\ \ \mu^{+}\left(z_{k}\right)-\Phi^{-1}\left(\beta\right)\sqrt{\Sigma^{+}}\ge x_{\min}\\
& \boldsymbol{x}_{e}\left(k|\ k\right)=\boldsymbol{x}_{e}\left(k\right),\ \ \boldsymbol{x}_{e}\left(k+i|\ k\right)=F\left(\boldsymbol{x}_{e}\left(k+i|\ k\right),\boldsymbol{u}\left(k+i|\ k\right)\right)\\
& \boldsymbol{x}\left(k+i|\ k\right)\in \mathrm{X},\ \ \boldsymbol{u}\left(k+i|\ k\right)\in \mathrm{U},\\
& v_{k+i|\ k}\in \mathrm{V}
\end{aligned}
$$

The cost function minimization problem is embedded into the receding-horizon optimization and recursive update process of MPC for online solution, thereby enabling real-time closed-loop control.

4. Simulation Validation

To verify the feasibility of the proposed MOGP-MPC method, numerical simulations were conducted on the MATLAB platform. A circular reference trajectory with a radius of 8 m was selected as the tracking target, and trajectory tracking control simulations were designed and implemented. The simulation settings are as follows: the initial position of the UUV is (8,0), and the initial heading angle is 0 rad; the sampling period is 0.1 s; the MPC prediction horizon is 12 steps; and the total simulation time is 160 s.

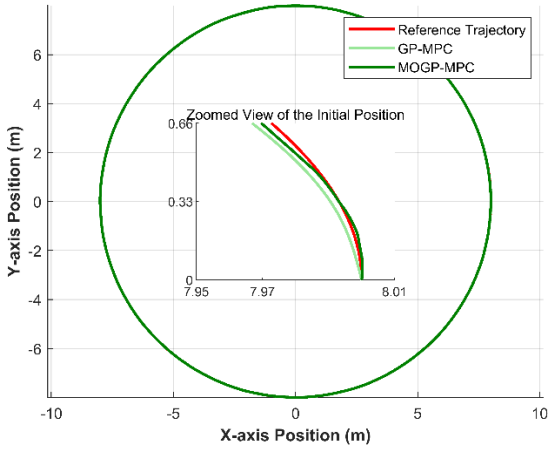

Figure 2. Comparative circular-trajectory tracking performance of GP-MPC and MOGP-MPC.

As shown in Fig. 2, a comparative study between GP-MPC and MOGP-MPC is conducted for the circular reference trajectory tracking task. The simulation results indicate that, in the presence of external disturbances and modeling errors, both control strategies are capable of achieving stable tracking of the circular reference trajectory for the UUV. This demonstrates that the constructed predictive control framework possesses a certain level of disturbance rejection capability and trajectory tracking feasibility. Meanwhile, a closer observation of the locally enlarged region reveals noticeable differences in tracking accuracy between the two methods. Compared with the conventional GP-MPC approach, the trajectory generated by MOGP-MPC more closely follows the reference trajectory with smaller deviations, indicating superior tracking performance and improved control accuracy under complex uncertain environments. Overall, these results validate the advantages of the multi-output Gaussian process model in capturing system coupling dynamics and compensating for unmodeled errors, thereby enhancing the robustness and stability of UUV trajectory tracking control.

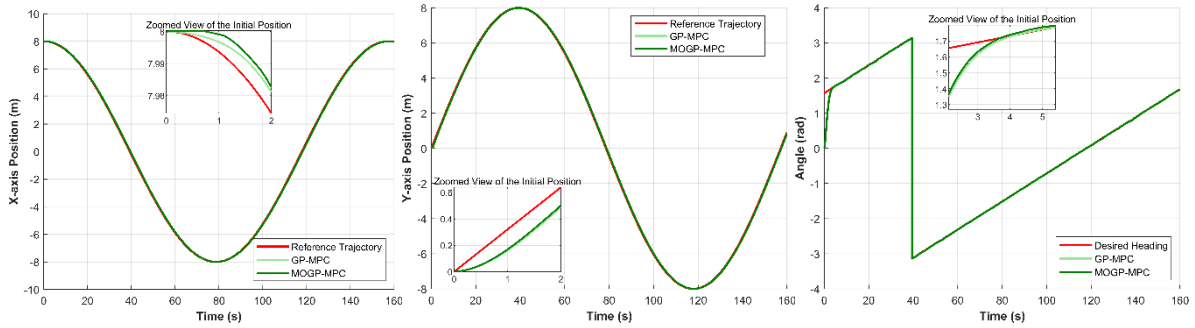

(a) (b) (c)

Figure 3. Comparison of planar pose tracking performance between GP-MPC and MOGP-MPC.

(a) X-axis Tracking Performance. (b) Y-axis Tracking Performance. (c) Heading Angle Tracking Performance.

The planar pose tracking results of the UUV are shown in Fig. 3. It can be observed that MOGP-MPC achieves higher tracking accuracy than GP-MPC in both the X- and Y-axis directions, as evidenced by position responses that are closer to the reference trajectory and smaller steady-state errors. Regarding heading angle control, both algorithms exhibit a certain degree of oscillation; however, each is capable of effectively tracking the desired heading and maintaining convergence. Overall, as illustrated in Fig. 3, MOGP-MPC demonstrates superior planar pose tracking performance and enhanced error suppression capability compared with GP-MPC, resulting in more stable control performance.

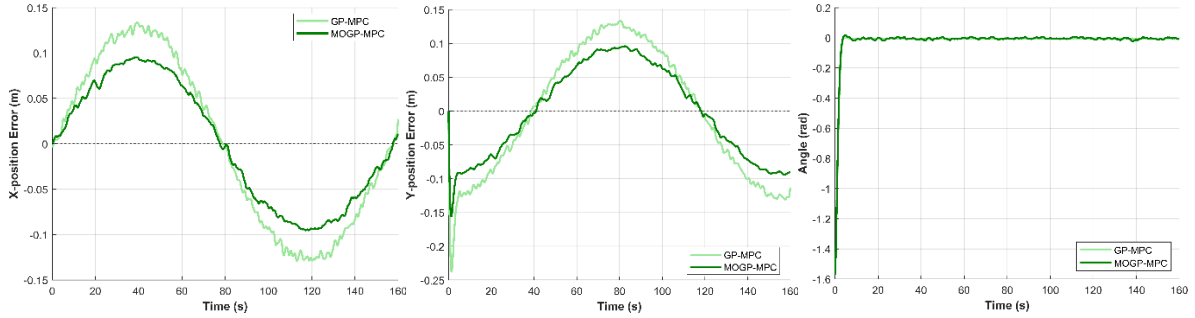

(a) (b) (c)

Figure 4. Comparison of planar pose tracking errors between GP-MPC and MOGP-MPC.

(a) X-axis Tracking Error. (b) Y-axis Tracking Error. (c) Heading Angle Tracking Error.

As shown in Fig. 4, the advantages of the MOGP-MPC control strategy are particularly evident. The tracking errors in both the X- and Y-axis directions remain consistently smaller than those of GP-MPC throughout the entire simulation process. Specifically, the tracking errors of MOGP-MPC along the X and Y directions are generally maintained within 0.1 m, whereas the errors of GP-MPC exceed 0.1 m on multiple occasions, exhibiting larger deviations and reduced stability. These results further demonstrate that, compared with GP-MPC, MOGP-MPC provides more significant improvements in error suppression and tracking accuracy.

5. Conclusion

This paper proposes a MOGP-MPC method for UUV trajectory tracking under model uncertainty and dynamic disturbances. By introducing ICM, the method compensates for modeling errors in each state channel while capturing the coupling relationships between states, thereby improving control accuracy and robustness. Experimental and simulation results demonstrate that, compared to the traditional single-output GP-MPC method, the proposed approach exhibits superior tracking

performance in multi-posture control tasks, especially when model uncertainty is present, significantly reducing errors and enhancing system stability. Additionally, by combining a stochastic constraint handling strategy based on GP prediction uncertainty, the overall system performance is further enhanced. The proposed MOGP-MPC method provides an effective solution for UUV trajectory tracking control, with significant research value and practical application potential. Future improvements will further advance UUV control technology, especially in complex and uncertain environments, demonstrating broad prospects.

References

[1] WANG N, GAO Y, ZHANG X. Data-driven performance-prescribed reinforcement learning control of an unmanned surface vehicle[J]. IEEE Transactions on Neural Networks and Learning Systems, 2021, 32(12):5456-5467.

[2] WANG N, GAO Y, ZHAO H, et al. Reinforcement learning-based optimal tracking control of an unknown unmanned surface vehicle[J]. IEEE Transactions on Neural Networks and Learning Systems, 2021, 32(7):3034-3045.

[3] PENG G, LU Z, TAN Z, et al. A novel algorithm based on nonlinear optimization for parameters calibration of wheeled robot mobile chasses[J]. Applied Mathematical Modelling, 2021, 95:396-408.

[4] YAN Z, YAN J, CAI S, et al. Robust MPC-based trajectory tracking of autonomous underwater vehicles with model uncertainty[J]. Ocean Engineering, 2023, 286:115617.

[5] DERINGER V L, BARTÓK A P, BERNSTEIN N, WILKINS D M, CERIOTTI M, CSÁNYI G. Gaussian process regression for materials and molecules[J]. Chemical Reviews, 2021, 121(16): 10073-10141.

[6] X. Yan and Y. Liu, "UUV Trajectory Tracking Control Based on Gaussian Process Model Predictive Control," 2024 3rd Conference on Fully Actuated System Theory and Applications (FASTA), Shenzhen, China, 2024. 1146-1151.

[7] SOLOPERTO R, KÖHLER J, ALLGÖWER F. Augmenting mpc schemes with active learning: Intuitive tuning and guaranteed performance[J]. IEEE Control Systems Letters, 2020, 4(3):713-718.

[8] XU X, CHEN H, LIAN C, et al. Learning-based predictive control for discrete-time nonlinear systems with stochastic disturbances[J]. IEEE Transactions on Neural Networks and Learning Systems, 2018, 29(12):6202-6213.

[9] AN Z, GONG P, ZHANG W, et al. Model predictive control of autonomous underwater vehicles for trajectory tracking with external disturbances[J]. Ocean Engineering, 2020, 217:107884.

[10] MORATO M M, FELIX M S. Data Science and Model Predictive Control: A survey of recent advances on data-driven MPC algorithms[J]. Journal of Process Control, 2024, 144: 103327.

[11] SUN D, JAMSHIDNEJAD A, DE SCHUTTER B. A novel framework combining MPC and deep reinforcement learning with application to freeway traffic control[J]. IEEE Transactions on Intelligent Transportation Systems, 2024, 25(7): 6756-6769.

[12] HEWING L, KABZAN J, ZEILINGER M N. Cautious model predictive control using gaussian process regression[J]. IEEE Transactions on Control Systems Technology, 2020, 28(6):2736-2743.

[13] A. P. Aguiar, A. M. Pascoal, Dynamic positioning and way-point tracking of underactuated AUVs in the presence of ocean currents, Proceedings of the 41st IEEE Conference on Decision and Control, (2002) 2105 2110.

[14] Qikun Shen, Peng Shi, Chee Peng Lim, Fuzzy adaptive fault-tolerant stability control against novel actuator faults and its application to me chanical systems, IEEE Transactions on Fuzzy Systems, 32 (4) (2024) 2331–2340.

[15] Wenjin Wang, Tao Wen, Xiao He, Guohua Xu, Robust trajectory tracking and control allocation of X-rudder AUV with actuator uncertainty, Control Engineering Practice, 136 (2023) 105535.

[16] L. Hewing, J. Kabzan, and M. N. Zeilinger, "Cautious model predictive control using gaussian process regression," IEEE Transactions on Control Systems Technology, vol. 28, no. 6, pp. 2736–2743, 2020.

[17] E. Schulz, M. Speekenbrink, and A. Krause, "A tutorial on gaussian process regression: Modelling, exploring, and exploiting functions," Journal of Mathematical Psychology, vol. 85, pp. 1–16, 2018.